Dynamic State Estimation of Medium-voltage DC Integrated Power System with Pulse Load

Runlong Xiao, Gang Wang, Xiaoliang Hao, Renji Huang, and Youxing Xiong

***Abstract*—The dynamic characteristic evaluation is an important prerequisite for safe and reliable operation of the medium-voltage DC integrated power system (MIPS), and the dynamic state estimation is an essential technical approach to the evaluation. Unlike the electromechanical transient process in a traditional power system, periodic change in pulse load of the MIPS is an electromagnetic transient process. As the system state suddenly changes in the range of a smaller time constant, it is difficult to estimate the dynamic state due to periodic disturbance. This paper presents a dynamic mathematical model of the MIPS according to the network structure and control strategy, thereby overcoming the restrictions of algebraic variables on the estimation and developing a dynamic state estimation method based on the extended Kalman filter. Using the method of adding fictitious process noise, it is possible to solve the problem that the linearized algorithm of the MIPS model is less reliable when an abrupt change occurs in the pulse load. Therefore, the accuracy of the dynamic state estimation and the stability of the filter can be improved under the periodic disturbance of pulse load. The simulation and experimental results confirm that the proposed model and method are feasible and effective.**

***Index Terms*—Medium-voltage DC integrated power system, pulse load, dynamic state estimation, extended Kalman filter, fictitious process noise.**

I. Introduction

THE vessel integrated power system means integrating the dynamical system of a traditional ship with its electrical system to provide electric energy for the propulsion system, shipborne equipment and daily service loads. It serves the function of central control and comprehensive utilization of energy sources, and it has advantages of improving the design of overall ship, increasing the system efficiency and reducing the noise. It was a trend towards information and intelligence [1], [2]. The medium-voltage DC transmission system is a completely new structure of power transmission network used in the integrated power system of a large vessel. It can further improve the efficiency and save the space while using the well-proven AC generators and motors, which is a trend of the structure of power transmission network in large ships. The main reason for the improved efficiency is that the system is no longer locked at a specific frequency. The medium-voltage DC transmission system is better than the medium-voltage AC transmission system because the transmission without reactive power can lessen the weight of the transmission cable, and the removal of large-capacity transformers can reduce the volume and weight of the power system greatly so as to optimize the overall design of a ship [3], [4]. The pulse load is a periodic high-power load released in a short time. Its pulse interval is a couple of seconds and its released power ranges from several hundred kilowatts to several megawatts, as is the case for radar, beam weapon and electromagnetic rail launcher [5]. Only the integrated power system can support the pulse load on board.

Dynamic state estimation is to use the data measured from multiple sections for estimating the system state variables, and the extended Kalman filter (EKF) is useful for the nonlinear system estimation with advantages of simple operation and quick calculation. As phasor measurement units and advanced communication facilities are widely used in power systems, it is possible to develop a fast-response and robust tool for dynamic state estimation. At present, the dynamic state estimation of land power system is mostly applied for the AC system and the optimal estimation of its linear ordinary differential equation [6] - [8]. In this system, when the load suddenly changes or the system is short-circuit, the dynamic change is small and slow compared with the scale of system capacity. This dynamic process is an electromechanical transient process and the time constant of the state equation is relatively large. The system will tend to be stable gradually. Sufficient dynamic state estimation methods are available for this system [9], [10]. As for the medium-voltage DC integrated power system (MIPS) which is a closely coupled AC/DC hybrid system, its diode switches alternatively perform a turn-on operation and a turn-off operation, therefore, its differential equation is time-varying. The state-space averaging method is used to eliminate the switching action to achieve a time-invariant model lending itself to system analysis and estimation. Further studies are needed to expand the state-space averaging model of synchronous generator with diode-bridge rectifier to the MIPS [11]. Besides,

Manuscript received: November 5, 2019; accepted: May 19, 2020. Date of CrossCheck: May 19, 2020. Date of online publication: June 25, 2020.

This work was supported by the National Key Basic Research Program of China (973 Program) (No. 613294) and the Natural Science Foundation of China (No. 51877211).

R. Xiao (corresponding author), G. Wang, X. Hao, R. Huang, and Y. Xiong are with the National Key Laboratory of Science and Technology on Vessel Integrated Power System, Naval University of Engineering, Wuhan 430033, China (e-mail: runlxiao@foxmail.com; wanggang6074@126.com; 18696174515@163.com; wuyingjituan@163.com; 2576641332@qq.com)

DOI: 10.35833/MPCE.2019.000145

the MIPS is a narrow and small system, so its load change is relatively large compared with its capacity, especially when its pulse load of high energy consumption directly enters the system, a great disturbance will appear in the system state. As a sudden change in the pulse load causes the system state to change abruptly in the range of a smaller time constant, in the periodic change of the pulse load, especially at the point of abrupt change of the load, a greater abrupt change will make a strong periodic impact on the MIPS. In the step change of system state variables such as voltage and current, the time constant becomes small. This process is a periodical electromagnetic transient process, and dynamic state estimation methods working on this system need further studies.

Studies on the MIPS and its estimation have just started. But most state estimation methods on an AC/DC hybrid system refer to the static state estimation at the present time [12]-[14]. As for the state estimation of MIPS, only an offline parameter estimation for tuning the controllers' linearizing function is founded [15], which refers to a static state estimation as well. In the existing literature, no studies on the dynamic state estimation of the MIPS have yet been found. The static state estimation methods cannot deal with the dynamics of the system in operation with pulse load. Dynamic state estimation is used instead of the static state estimation because it can better estimate the dynamic characteristics of the system state, and will play an important role in the control and protection of power systems. Compared with the dynamic state of the traditional land power systems which tends to be stable after disturbance, the dynamic disturbance will greatly affect the estimated effect of the filter when the MIPS operates with its pulse load changing periodically [5], [15]. A periodic change in the pulse load of the MIPS may cause trouble for the linearized algorithm of the system model, and the adaptability of the EKF to the MIPS needs to be studied. Hence, there is a need for a dynamic mathematical model describing its dynamic change.

In this paper, a mathematical model of the MIPS is established according to the topology of the system and the control strategy of the equipment, and a dynamic state estimation method is proposed based on the EKF, thereby solving the problem of algebraic variables on the estimation. The addition of fictitious process noise (FPN) to the system model at the point of abrupt change of the pulse load will improve the estimation accuracy and the filter stability under the periodic disturbance. The simulation and experimental results prove the effectiveness of the model and algorithm.

II. Structure and Mathematical Model of MIPS

A. Structure of MIPS

Figure 1 shows a typical network structure of the MIPS [16]. Its m prime movers including gas turbines and diesels drive a group of three-phase synchronous generators (G1-Gm) to generate AC, which is transformed into DC after uncontrolled rectification. The generators connected in parallel supply DC to the DC busbar, and the DC busbar provides the pulse load, the propulsion load and the daily service load with electricity. There is a filter capacitor and filter inductors at the end of the rectifiers. The high-speed excitation system keeps the output DC voltage of the rectifier generators constant and controls their power outputs.

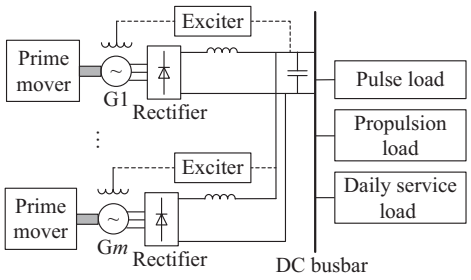

Fig. 1. Structure of MIPS.

The pulse load is connected to the DC busbar directly and releases a large amount of power during a short period, which makes strict demands on the vessel power system. The operation characteristics of the pulse load are shown in Fig. 2. The first kind is a rectangular-wave pulse load, as shown in Fig. 2(a). The operation characteristic of pulse power P_L is a rectangular wave in a period of T, in which the maximum power is P_h and the minimum power is $P_l=0$, with the time of their actions being equal [17]. The second kind is a triangular-wave pulse load, as shown in Fig. 2(b). Its pulse power P_L is a periodic ramp function, which rises from $P_l=0$ to P_h in a period of T. The load operates in the form of triangular wave [18].

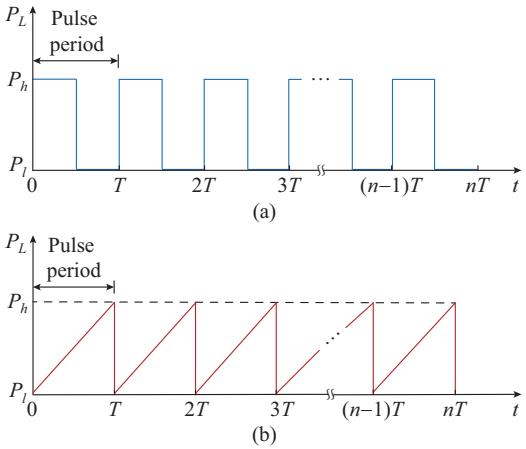

Fig. 2. Characteristics of pulse load. (a) Rectangular-wave pulse load. (b) Triangular-wave pulse load.

B. Mathematical Model of MIPS

It is necessary to establish a mathematical model for the equivalent load circuit of the MIPS. As shown in Fig. 3, R is the resistive load of the MIPS; $P=P_L+P_C$ is the operation power of the MIPS with the power of propulsion load P_C equivalent to P_L; I_1 is the output current; C is the filter capacitance; and E_{dc} and I_{dc} are the voltage and the total output current of the DC busbar, respectively.

By Kirchhoff's Law, the state equation of DC voltage in the equivalent load is written in per-unit value as follow:

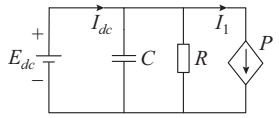

Fig. 3. Equivalent load circuit of MIPS.

$$pE_{dc}=\frac{1}{T'_{RC}}\left(I_{dc}R-\frac{3P}{2E_{dc}}R-E_{dc}\right) \tag{1}$$

where p is the derivative, p=d/dt. If the peak values of the rated AC voltage and current of the generator are chosen as the base quantities, the term 3/2 in (1) is the calculated result of P [19], and the time constant is $T'_{RC}=RC$.

There is a need to establish a mathematical model of the excitation system of the generator group. To keep the DC busbar voltage constant and make the rectifier generators produce the output power according to the ratio of their rated power, the excitation system uses the traditional droop control strategy to control the output power. As the droop control does not depend on the designated main generator to regulate the voltage, it is possible to prevent the system from breaking down due to a fault in the main generator in a master-slave control mode, and meanwhile, to decrease its dependency on the communication system and improve the reliability of the transmission system [20]. When the high-speed exciters are used, the time delay of excitation control can be ignored. Assume that the rated DC current of i^{th} ($i=1,2,\ldots,m$) rectifier generator in the system is I_{dcri}, the output current of the i^{th} rectifier generator is I_{dci}, the rated voltage of DC busbar is E_{dcr}, and the voltage regulation rate of DC busbar is 2α. By combining E_{dc} with I_{dci} of each generator linearly and comparing that with the intercept coefficient E_{dc0} of the excitation system, the control law of the system in the steady state is as follows:

$$E_{dc}+k_iI_{dci}=E_{dc0}\quad i=1,2,...,m \tag{2}$$

where k_i is the droop coefficient of the excitation system in the i^{th} generator, or the linear coefficient of output current. According to the voltage regulation rate, when the rectifier generator operates with no load (I_{dci}=0), E_{dc} is equal to $E_{dcr}(1+\alpha)$, thus $E_{dc0}=E_{dcr}(1+\alpha)$. When the rectifier generator operates with the rated load (I_{dci}=I_{dcri}), E_{dc} is equal to $E_{dcr}(1-\alpha)$. Hence, k_i and E_{dc0} are calculated as follows:

$$\begin{cases}k_i=\dfrac{2\alpha E_{dcr}}{I_{dcri}} & i=1,2,...,m\\ E_{dc0}=E_{dcr}(1+\alpha)\end{cases} \tag{3}$$

The result of $I_{dc1}:I_{dc2}:\ldots:I_{dcm}=I_{dcr1}:I_{dcr2}:\ldots:I_{dcrm}$ can be calculated by (2) and (3). It means that the parallel rectifier generators will output the power according to their ratio of rated power. Figure 4 shows the excitation system under the droop control.

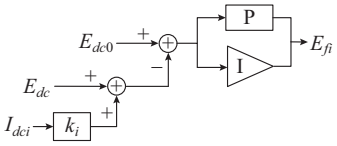

Fig. 4. Excitation system under droop control.

According to the control law expressed in (2), the difference between $E_{dc}+k_iI_{dci}$ and E_{dc0} goes through the proportional-integral (PI) controller and produces the excitation voltage E_{fi}, which can keep the DC voltage constant and make the output power of the rectifier generators distributed equally according to their rated capacity. For the i^{th} generator, k_{1i} and k_{2i} are the proportional and integral coefficients of the PI controller, respectively; and x_i is the integral output of the PI controller. For $i=1,2,\ldots,m$, the state equations of E_{fi} and x_i are as follows:

$$\begin{cases}E_{fi}=k_{1i}\left[E_{dc0}-(E_{dc}+k_iI_{dci})\right]+k_{2i}x_i\\ px_i=E_{dc0}-(E_{dc}+k_iI_{dci})\end{cases} \tag{4}$$

In [5], [21], the rectification of the generator is equivalent to that of the voltage source, which shows a process of conduction and commutation. The model is obtained after state-space averaging. The principle of harmonic balance is applied to construct a state-space mathematical model of a synchronous generator with diode-bridge rectifier. For $i=1,2,\ldots,m$, the state-space model of the MIPS is expressed as (4)-(15).

$$pE'_{qi}=\frac{1}{T'_{d0i}}\left[E_{fi}-(x_{di}-x'_{di})\bar{i}_{di}-E'_{qi}\right] \tag{5}$$

$$pE'_{di}=\frac{1}{T'_{q0i}}\left[(x_{qi}-x'_{qi})\bar{i}_{qi}-E'_{di}\right] \tag{6}$$

$$pI_{dci}=\frac{1}{r_{dci}T'_{dci}}\left\{\frac{3\sqrt{3}}{\pi}E_{1i}-\left[\frac{3x_{ti}}{\pi}+\left(2-\frac{3u_i}{2\pi}\right)r_i+r_{dci}\right]I_{dci}-E_{dc}\right\} \tag{7}$$

$$pE_{dc}=\frac{1}{T'_{RC}}\left(\sum_{i=1}^{m}I_{dci}R-\frac{3P}{2E_{dc}}R-E_{dc}\right) \tag{8}$$

$$E_{1i}=\sqrt{\left[E'_{qi}-(x'_{di}-x''_{di})\bar{i}_{di}\right]^2+\left[E'_{di}+(x'_{qi}-x''_{qi})\bar{i}_{qi}\right]^2} \tag{9}$$

$$\delta_i=\tan^{-1}\frac{E'_{di}+(x'_{qi}-x''_{qi})\bar{i}_{qi}}{E'_{qi}-(x'_{di}-x''_{di})\bar{i}_{di}} \tag{10}$$

$$\bar{i}_{di}=\frac{\sqrt{3}}{\pi}\frac{\sqrt{\sin^2(\mu_i)+\mu_i^2-\mu_i\sin(2\mu_i)}}{1-\cos(\mu_i)}I_{dci}\sin(\delta_i+\varphi_i) \tag{11}$$

$$\bar{i}_{qi}=\frac{\sqrt{3}}{\pi}\frac{\sqrt{\sin^2(\mu_i)+\mu_i^2-\mu_i\sin(2\mu_i)}}{1-\cos(\mu_i)}I_{dci}\cos(\delta_i+\varphi_i) \tag{12}$$

$$\mu_i=\cos^{-1}\left(1-\frac{2x_{ti}I_{dci}}{\sqrt{3}\,E_{1i}}\right) \tag{13}$$

$$T'_{dci}=\frac{x_{dci}+\left(2-\dfrac{3\mu_i}{2\pi}\right)x_{ti}}{r_{dci}} \tag{14}$$

$$\varphi_i=\tan^{-1}\frac{2\mu_i-\sin(2\mu_i)}{1-\cos(2\mu_i)} \tag{15}$$

where $\sum_{i=1}^{m}I_{dci}=I_{dc}$; T'_{d0i} and T'_{q0i} are the transient open-circuit

time constants of the generator in *d*- and *q*-axes, respectively; T'_{dci} is the time constant of the rectifier circuit; E'_{di} and E'_{qi} are the transient voltages of the generator in *d*- and *q*-axes, respectively; $\bar{i}_{di}$ and $\bar{i}_{qi}$ are the currents of the generator in *d*- and *q*-axes, respectively; x_{di} and x_{qi} are the reactance of the generator in *d*- and *q*-axes, respectively; x'_{di} and x'_{qi} are the transient reactance of the generator in *d*- and *q*-axes, respectively; x''_{di} and x''_{qi} are the sub-transient reactance of the generator in *d*- and *q*-axes, respectively; $x_{ti}=(x''_{di}+x''_{qi})/2$ is the commutation reactance; r_i is the stator resistance; r_{dci} and x_{dci} are the equivalent rectification resistance and reactance, respectively; E_{1i} is the equivalent voltage; and μ_i, δ_i and φ_i are the commutation conduction angle, the phase angle of the equivalent voltage, and the phase angle between the current and the voltage, respectively.

Equations (4) - (15) represent the mathematical model of the MIPS, and the rank *n* observability matrix derived by the method based on the Lie derivatives [7] indicates that the system is observable.

The 4*m*+1 dimensional state variable vector $\boldsymbol{x}$ and the 7*m* dimensional algebraic variable vector $\boldsymbol{y}$ of the system are: $\boldsymbol{x}=[E'_{d1},E'_{q1},i_{dc1},x_1,...,E'_{dm},E'_{qm},i_{dcm},x_m,E_{dc}]^{\mathrm{T}}$; $\boldsymbol{y}=[E_1,\delta_1,\bar{i}_{d1},\bar{i}_{q1},\mu_1,E_{f1},\varphi_1,...,E_m,\delta_m,\bar{i}_{dm},\bar{i}_{qm},\mu_m,E_{fm},\varphi_m]^{\mathrm{T}}$. Thus, the differential-algebraic equations (4)-(15) can be expressed in matrix form as follows:

$$\begin{cases} p\boldsymbol{x}=\boldsymbol{f}(\boldsymbol{x},\boldsymbol{y}) \\ \boldsymbol{0}=\boldsymbol{g}(\boldsymbol{x},\boldsymbol{y}) \end{cases} \tag{16}$$

III. Dynamic State Estimation Method of MIPS

A. EKF-based Method

There are some difficulties in the direct application of Kalman filter to the state-space model expressed by (4) - (15). This is because most of the state variables are fictitious and immeasurable, and the state equation of the model contains quite a few algebraic variables. In (4) - (15), algebraic variables are quite complex because they involve the correlation between the state variables and the correlation between the algebraic variables, which will lead the state equation to be of strong nonlinearity. The EKF is a fundamental approach for the estimation of the nonlinear system, which can be used to estimate the dynamic state of the MIPS in this paper. The basic principle of EKF is to obtain the predicted value of state variable at the next moment from the linearized state equations and use the measured value to modify the predicted value [6]. For the dynamic state estimation, it is necessary to eliminate the constraint of algebraic variables when the nonlinear continuous system is turned into a linear discrete system. As for a large number of algebraic variables in the model, the state equations and algebraic equations are linearized, the algebraic terms are incorporated and removed, and their values are updated along with the state variables in real time. According to [6], the estimation method based on the EKF is described as follows.

1) Euler's formula is often used to convert the differential-algebraic equation (16) into the discrete equation as follows:

$$\begin{cases} \boldsymbol{x}_k=\boldsymbol{x}_{k-1}+h\boldsymbol{f}(\boldsymbol{x}_{k-1},\boldsymbol{y}_{k-1},\boldsymbol{w}_{k-1}) \\ \boldsymbol{0}=\boldsymbol{g}(\boldsymbol{x}_{k-1},\boldsymbol{y}_{k-1}) \end{cases} \tag{17}$$

where the subscript *k* is the position of the estimation point; $\boldsymbol{w}_{k-1}$ is the process noise; and $h=\Delta t$ is the time step. The smaller the time step is, the higher accuracy the filter has.

Thus, the state estimation model can be expressed as:

$$\begin{cases} \boldsymbol{x}_k=\boldsymbol{x}_{k-1}+h\boldsymbol{f}(\boldsymbol{x}_{k-1},\boldsymbol{y}_{k-1},\boldsymbol{w}_{k-1}) \\ \boldsymbol{0}=\boldsymbol{g}(\boldsymbol{x}_{k-1},\boldsymbol{y}_{k-1}) \\ \boldsymbol{z}_k=\boldsymbol{h}(\boldsymbol{x}_k,\boldsymbol{v}_k) \\ \boldsymbol{w}_k\sim(\boldsymbol{0},\boldsymbol{Q}_k) \\ \boldsymbol{v}_k\sim(\boldsymbol{0},\boldsymbol{R}_k) \end{cases} \tag{18}$$

where $\boldsymbol{z}_k$ is the measurement equation; $\boldsymbol{v}_k$ is the measurement noise whose mean value is zero; and $\boldsymbol{Q}_k$ and $\boldsymbol{R}_k$ are the positively definite covariance matrices.

2) Taylor's series expansion of the state equation is carried out around $(\boldsymbol{x}^+_{k-1},\boldsymbol{y}^+_{k-1})$ and $\boldsymbol{w}_{k-1}=\boldsymbol{0}$ to obtain the following:

$$\begin{cases} \boldsymbol{x}_k=\boldsymbol{x}_{k-1}+h[\boldsymbol{f}(\boldsymbol{x}^+_{k-1},\boldsymbol{y}^+_{k-1},0)+\boldsymbol{A}_{k-1}(\boldsymbol{x}_{k-1}-\boldsymbol{x}^+_{k-1})+ \\ \qquad \boldsymbol{B}_{k-1}(\boldsymbol{y}_{k-1}-\boldsymbol{y}^+_{k-1})+\boldsymbol{L}_{k-1}\boldsymbol{w}_{k-1}] \\ \boldsymbol{0}=\boldsymbol{g}(\boldsymbol{x}^+_{k-1},\boldsymbol{y}^+_{k-1})+\boldsymbol{C}_{k-1}(\boldsymbol{x}_{k-1}-\boldsymbol{x}^+_{k-1})+\boldsymbol{D}_{k-1}(\boldsymbol{y}_{k-1}-\boldsymbol{y}^+_{k-1}) \end{cases} \tag{19}$$

where the superscript + represents the posteriori estimation; $\boldsymbol{A}_{k-1}=\partial\boldsymbol{f}/\partial\boldsymbol{x}\big|_{(\boldsymbol{x}^+_{k-1},\boldsymbol{y}^+_{k-1})}$; $\boldsymbol{B}_{k-1}=\partial\boldsymbol{f}/\partial\boldsymbol{y}\big|_{(\boldsymbol{x}^+_{k-1},\boldsymbol{y}^+_{k-1})}$; $\boldsymbol{C}_{k-1}=\partial\boldsymbol{g}/\partial\boldsymbol{x}\big|_{(\boldsymbol{x}^+_{k-1},\boldsymbol{y}^+_{k-1})}$; $\boldsymbol{D}_{k-1}=\partial\boldsymbol{g}/\partial\boldsymbol{y}\big|_{(\boldsymbol{x}^+_{k-1},\boldsymbol{y}^+_{k-1})}$; and $\boldsymbol{L}_{k-1}=\partial\boldsymbol{f}/\partial\boldsymbol{w}\big|_{(\boldsymbol{x}^+_{k-1},\boldsymbol{y}^+_{k-1})}$.

Because $\boldsymbol{g}(\boldsymbol{x}^+_{k-1},\boldsymbol{y}^+_{k-1})=\boldsymbol{0}$, the incorporation of the two in (19) and the elimination of the item $\boldsymbol{y}_{k-1}-\boldsymbol{y}^+_{k-1}$ lead to:

$$\boldsymbol{x}_k=\boldsymbol{F}_{k-1}\boldsymbol{x}_{k-1}+\hat{\boldsymbol{u}}_{k-1}+\hat{\boldsymbol{w}}_{k-1}$$

where $\boldsymbol{F}_{k-1}=\boldsymbol{I}+h(\boldsymbol{A}_{k-1}-\boldsymbol{B}_{k-1}\boldsymbol{D}^{-1}_{k-1}\boldsymbol{C}_{k-1})$, and $\boldsymbol{I}$ is the unit matrix. The known signal $\hat{\boldsymbol{u}}_{k-1}$ and the noise signal $\hat{\boldsymbol{w}}_{k-1}$ are defined as:

$$\begin{cases} \hat{\boldsymbol{u}}_{k-1}=h[\boldsymbol{f}(\boldsymbol{x}^+_{k-1},\boldsymbol{y}^+_{k-1},\boldsymbol{0})-(\boldsymbol{A}_{k-1}-\boldsymbol{B}_{k-1}\boldsymbol{D}^{-1}_{k-1}\boldsymbol{C}_{k-1})\boldsymbol{x}^+_{k-1}] \\ \hat{\boldsymbol{w}}_{k-1}\sim(\boldsymbol{0},\boldsymbol{L}_{k-1}\boldsymbol{Q}_{k-1}\boldsymbol{L}^{\mathrm{T}}_{k-1}) \end{cases} \tag{20}$$

3) With $\boldsymbol{E}$ representing the expected value, the initialization of the filter and the estimation error covariance can be expressed as follows:

$$(\boldsymbol{x}^+_0,\boldsymbol{y}^+_0)=\boldsymbol{E}(\boldsymbol{x}_0,\boldsymbol{y}_0) \tag{21}$$

$$\boldsymbol{P}^+_0=\boldsymbol{E}((\boldsymbol{x}_0-\boldsymbol{x}^+_0,\boldsymbol{y}_0-\boldsymbol{y}^+_0)(\boldsymbol{x}_0-\boldsymbol{x}^+_0,\boldsymbol{y}_0-\boldsymbol{y}^+_0)^{\mathrm{T}}) \tag{22}$$

4) For $k=1,2,...,n$, it is necessary to take the following steps.

Step 1: calculate the partial derivative matrices.

$$\boldsymbol{F}_{k-1}=\boldsymbol{I}+h(\boldsymbol{A}_{k-1}-\boldsymbol{B}_{k-1}\boldsymbol{D}^{-1}_{k-1}\boldsymbol{C}_{k-1})\big|_{(\boldsymbol{x}^+_{k-1},\boldsymbol{y}^+_{k-1})} \tag{23}$$

Step 2: perform the time update of the state estimation and estimation error covariance matrices.

$$\begin{cases} \boldsymbol{x}^-_k=\boldsymbol{x}^+_{k-1}+h\boldsymbol{f}(\boldsymbol{x}^+_{k-1},\boldsymbol{y}^+_{k-1},\boldsymbol{0}) \\ \boldsymbol{P}^-_k=\boldsymbol{F}_{k-1}\boldsymbol{P}^+_{k-1}\boldsymbol{F}^{\mathrm{T}}_{k-1}+\boldsymbol{L}_{k-1}\boldsymbol{Q}_{k-1}\boldsymbol{L}^{\mathrm{T}}_{k-1} \end{cases} \tag{24}$$

where the superscript − represents the priori estimation.

Step 3: linearize the measurement equation $\boldsymbol{z}_k=\boldsymbol{h}(\boldsymbol{x}_k,\boldsymbol{v}_k)$ around $\boldsymbol{x}^-_k$ and $\boldsymbol{v}_k=\boldsymbol{0}$ and calculate the matrices

$\boldsymbol{H}_k = \partial \boldsymbol{h}/\partial \boldsymbol{x}\big|_{\boldsymbol{x}_k^-}$, $\boldsymbol{M}_k = \partial \boldsymbol{h}/\partial \boldsymbol{v}\big|_{\boldsymbol{x}_k^-}$.

Step 4: perform the measurement update of the state estimation and estimation error covariance matrices.

$$\begin{cases} \boldsymbol{K}_k = \boldsymbol{P}_k^- \boldsymbol{H}_k^{\mathrm{T}} (\boldsymbol{H}_k \boldsymbol{P}_k^- \boldsymbol{H}_k^{\mathrm{T}} + \boldsymbol{M}_k \boldsymbol{R}_k \boldsymbol{M}_k)^{-1} \\ \boldsymbol{x}_k^+ = \boldsymbol{x}_k^- + \boldsymbol{K}_k (\boldsymbol{z}_k - \boldsymbol{h}(\boldsymbol{x}_k^-, \boldsymbol{0})) \\ \boldsymbol{P}_k^+ = (\boldsymbol{I} - \boldsymbol{K}_k \boldsymbol{H}_k) \boldsymbol{P}_k^- \end{cases} \tag{25}$$

Step 5: take $\boldsymbol{y}_{k-1}^+$ as an initial variable for the estimated value $\boldsymbol{x}_k^+$, and use the Newton iteration method to solve the algebraic equation $\boldsymbol{g}(\boldsymbol{x}_k^+, \boldsymbol{y}_k^+) = \boldsymbol{0}$ so as to update the algebraic variable $\boldsymbol{y}_k^+$. The steps include: ① solve the residual error $\boldsymbol{dg} = \boldsymbol{g}(\boldsymbol{x}_k^+, \boldsymbol{y}_{k-1}^+)$ and Jacobian matrix $\boldsymbol{G} = \partial \boldsymbol{g}/\partial \boldsymbol{y}\big|_{\boldsymbol{y}_{k-1}^+}$; ② modify the algebraic variable $\boldsymbol{y}_k^+ = \boldsymbol{y}_{k-1}^+ - \boldsymbol{G}^{-1} \cdot \boldsymbol{dg}$; ③ use the modified algebraic variables and repeat the above two steps until each element in $\boldsymbol{dg}$ reaches the given accuracy.

B. Fictitious Process Noise

According to (24), the EKF depends on the currently estimated value to predict the state variables at the next moment, and the use of Euler method to discretize the differential equations for state prediction is to take the first two terms out of the Taylor series expansion at the point $(\boldsymbol{x}_{k-1}^+, \boldsymbol{y}_{k-1}^+)$ [19]. But when there are discontinuous derivatives at the point of abrupt change of the pulse load , the error in (24) is large because the derivability near the expansion point is a precondition of Taylor series expansion. In other words, the power produced from the sudden-change pulse load will greatly change the system state. In (24), there is a relatively large error between the predicted value obtained from the currently estimated value and the actual value, which will affect the following calculation. Hence, the linearized algorithm of the system model in (24) is considered to be less reliable when an abrupt change occurs in the pulse load.

At this point, the addition of FPN makes the EKF focus on the measurements but not the system model in the abrupt change of pulse load. After a short-time iteration, the system model becomes reliable again, and the FPN is removed to improve the filter performance. According to the theoretical analysis of the compensation for modeling errors by the FPN in Section 5.5 of [6], the concise proof is as follows.

1) If $\boldsymbol{Q}_{k-1}$ in (24) is small, the covariance may not increase much between time samples. In the example 5.3 of [6], $\boldsymbol{F}_{k-1} = \boldsymbol{1}$, so $\boldsymbol{P}_k^- = \boldsymbol{P}_{k-1}^+$ when $\boldsymbol{Q}_{k-1} = \boldsymbol{0}$. However, whenever a measured value is obtained, the covariance will drop from $\boldsymbol{P}_k^-$ down to $\boldsymbol{P}_k^+$ according to the equation of measurement update for the covariance. Eventually $\boldsymbol{P}_k^-$ will converge to zero. Replacing $\boldsymbol{P}_{k-1}^+$ in (24) with $\boldsymbol{P}_{k-1}^+$ in (25) can obtain the one-step equation for $\boldsymbol{P}_k^-$:

$$\boldsymbol{P}_k^- = \boldsymbol{F}_{k-1} \boldsymbol{P}_{k-1}^- \boldsymbol{F}_{k-1}^{\mathrm{T}} - \boldsymbol{F}_{k-1} \boldsymbol{K}_{k-1} \boldsymbol{H}_{k-1} \boldsymbol{P}_{k-1}^- \boldsymbol{F}_{k-1}^{\mathrm{T}} + \boldsymbol{L}_{k-1} \boldsymbol{Q}_{k-1} \boldsymbol{L}_{k-1}^{\mathrm{T}} \tag{26}$$

2) If $\boldsymbol{Q}_{k-1} = \boldsymbol{0}$, the steady solution of (26) is zero. As shown in (25), the zero value of $\boldsymbol{P}_k^-$ will result in $\boldsymbol{K}_k$=$\boldsymbol{0}$. The zero value of $\boldsymbol{K}_k$ means that the equation for $\boldsymbol{x}_k^+$ in (25) will not involve any measured value. The measured value $\boldsymbol{z}_k$ will be completely ignored in the computation of $\boldsymbol{x}_k^+$. That is because the measurement noise covariance $\boldsymbol{R}_k$ (assumed to be greater than zero) will always be larger than the process noise $\boldsymbol{Q}_{k-1} = \boldsymbol{0}$. The insensitivity of the filter to the measured value will lead to the sluggish response of the filter.

3) If $\boldsymbol{Q}_{k-1}$ is large, then the covariance will constantly increase between time samples, that is, $\boldsymbol{P}_k^-$ will always be larger than $\boldsymbol{P}_{k-1}^+$. When converging, $\boldsymbol{P}_k^-$ will converge to a larger value, which will make $\boldsymbol{K}_k$ converge to a larger value as well. Here, $\boldsymbol{K}_k$ with larger value means that the measurement update for $\boldsymbol{x}_k^+$ in (25) will include a more important measured value, on which the filter will put greater emphasis.

IV. Simulation Analysis

A. Analysis on Mathematical Model of MIPS

To verify the proposed mathematical model, a turbine generator unit and a diesel generator unit are used as an example. A simulation model and a mathematical model are built in PSCAD/EMTDC. The diagrams of the simulation model and the control system of generator are shown in Figs. 5 and 6, respectively.

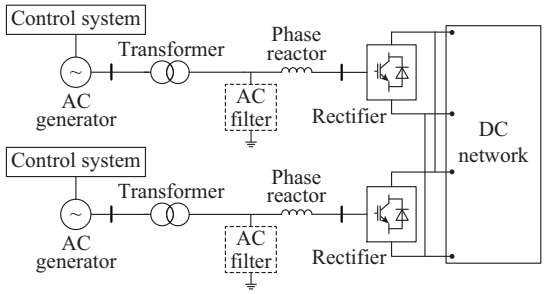

Fig. 5. Diagram of simulation model.

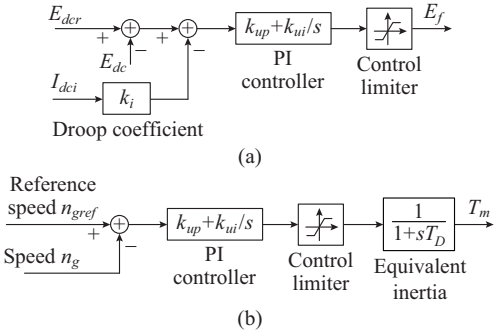

Fig. 6. Diagram of control system of generator. (a) Excitation control. (b) Speed control.

The rated capacities of the two generators are 24 MW and 6 MW, respectively, whose droop coefficients are 0.085 and 0.340, respectively, and $\alpha = 0.02$. The base values of voltage and current of the 24 MW generator (the 1st generator) are 5656.9 V and 2828.4 A, respectively, and those of the 6 MW generator (the 2nd generator) are 5656.9 V and 707.1 A, respectively. The other parameters of the two generators are identical in per-unit value when their base values are used in the calculation. The parameters are listed in Table I. Considering the overall MIPS, the base values of the 24 MW generator are valid.

TABLE I
PARAMETERS OF MIPS

T'_{d0i}	T'_{q0i}	T'_{RC}	x_{di}	x'_{di}	x''_{di}	x_{ti}	x_{qi}
0.491	0.850	0.034	2.4	0.108	0.072	0.072	1.920
x'_{qi}	x''_{qi}	r_{dci}	r_i	k_{1i}	k_{2i}	x_{dci}	
0.228	0.072	0.03	0.051	5	4	0.3	

To verify these two models, it is necessary to analyze the dynamic characteristic of the system when an abrupt change occurs in the load. The rated voltage of the DC busbar E_{dcr} is 6000 V. The resistive load is $R=6\ \Omega$. The operation power P suddenly drops from 9 MW to 3 MW at 10 s. Figure 7 (a) and (b) shows the waveforms of E_{dc} and the output DC current I_{dc1} of the 24 MW generator in that transient process.

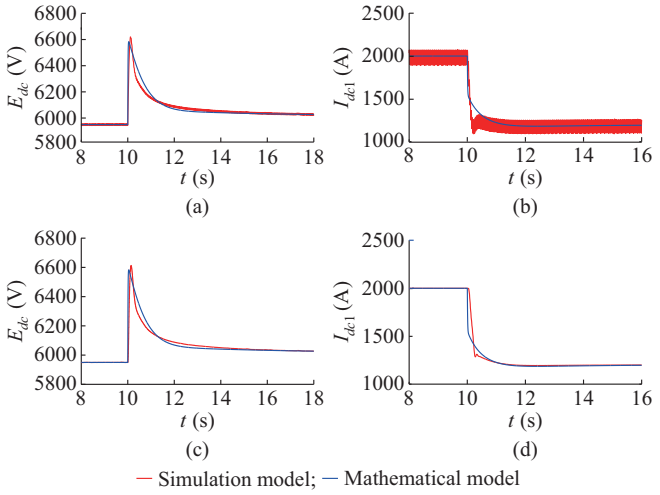

Fig. 7. Dynamic characteristics of MIPS during abrupt change of load. (a) Voltage of two models. (b) Current of two models. (c) DC component of voltage of two models. (d) DC component of current of two models.

Reference [22] presents that the mathematical model built on the state-space equations is used to describe the DC component of the state variables, namely the periodic mean value. The test result of the simulation model in Fig. 7(a) and (b) takes the form of periodic ripple, and it needs Fourier decomposition to get the DC component, as shown in Fig. 7(c) and (d). It is obvious that the result of the mathematical model is in an agreement with that of the simulation model, which shows that the mathematical model can accurately describe the dynamic characteristics of the MIPS during the abrupt change of the load.

The operation power P is 3 MW, but the other parameters are kept unchanged. To verify the dynamic characteristic of the system during the sudden change of the DC busbar voltage, the E_{dcr} controlled by the excitation system can be assumed to rise from 5000 V to 6000 V suddenly at 10 s. Figure 8(a) and (b) shows the outcome produced in the transient process. Figure 8(c) and (d) shows the result of the DC components. The results obtained from the two models are almost the same in the transient process. Thus, the mathematical model is capable of correctly describing the dynamic characteristics of the MIPS with a sudden change in its DC voltage.

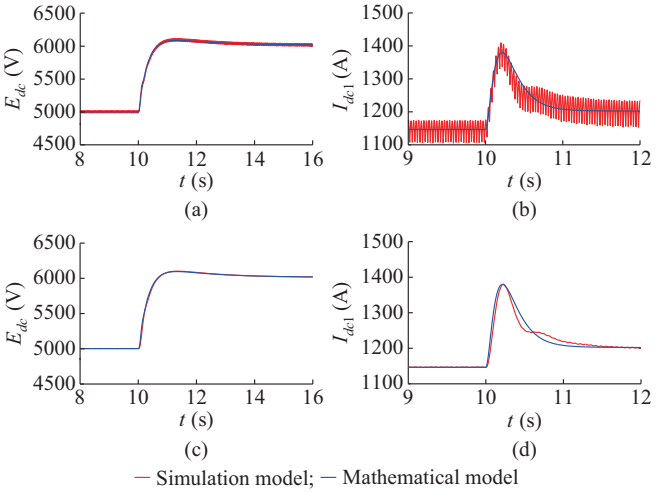

Fig. 8. Dynamic characteristics of MIPS during abrupt change of DC voltage controlled by excitation system. (a) Voltage of two models. (b) Current of two models. (c) DC component of voltage of two models (d) DC component of current of two models.

According to the comparison of the above-mentioned results, both the models produce almost the same results in a steady state. But with the transient errors within the permissible range of engineering application, the mathematical model is accurate enough to describe the dynamic characteristics, so it can be used for dynamic state estimation.

B. Dynamic State Estimation

The method based on the EKF is adopted for the dynamic state estimation. The measurement vector is $[E_{f1}, E_{f2}, I_{dc1}, I_{dc2}, E_{dc}]$. Equation (4) shows that E_{fi} is a linear combination of state variables I_{dci}, E_{dc} and x_i, and thus the measurement equation does not need to be linearized. Assuming that the measurement sensor makes the measured value have 1% Gauss white noise based on its true value, the initial value of the covariance matrix of measurement noise is $\boldsymbol{R}_0=10^{-4}\boldsymbol{I}_5$, $\boldsymbol{I}_5$ denoting a 5-dimension unit matrix. Based on the tests in Section III, the parameters remain unchanged and h is 5 ms. For the two kinds of pulse load, when the load power $P_l=0$, $P_h=0.375$, the period $T=10$ s and $P_C=0.125$, the minimum power of the equivalent load is $P_{\min}=0.125$ and the maximum power is $P_{\max}=0.5$. Thus, the power change P_m in the sudden-change pulse load is $P_{\max}-P_{\min}=0.375$.

The initial value of the EKF is based on the information obtained in advance. The closer it is to the true value, the faster the filter converges. The initial values of state and algebra variables are determined as the steady solution worked out by the mathematical model. The initial value of the covariance matrix of estimation error is $\boldsymbol{P}_0=0.01\boldsymbol{I}_9$ and the initial value of the covariance matrix of process noise is $\boldsymbol{Q}_0=10^{-6}\boldsymbol{I}_9$. The Section 13.1 in [6] shows that the value of P is obtained from the measurement. It contains a zero-mean random variable ΔP, whose variance is 0.01^2 and is used as part of the process noise. Taking the 1st generator for example, the estimated results of E_{dc} and I_{dc1} are shown in Figs. 9 and 10 and other state variables are shown in Figs. 11 and 12.

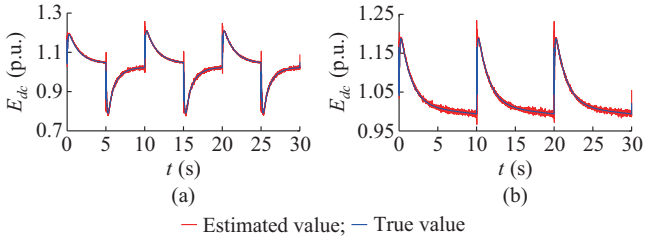

Fig. 9. DC busbar voltage of MIPS. (a) Under rectangular-wave pulse load. (b) Under triangular-wave pulse load.

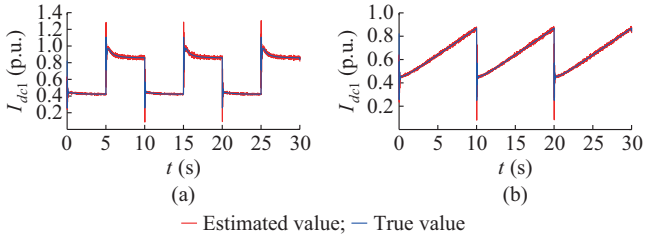

Fig. 10. Output current of 1st generator. (a) Under rectangular-wave pulse load. (b) Under triangular-wave pulse load.

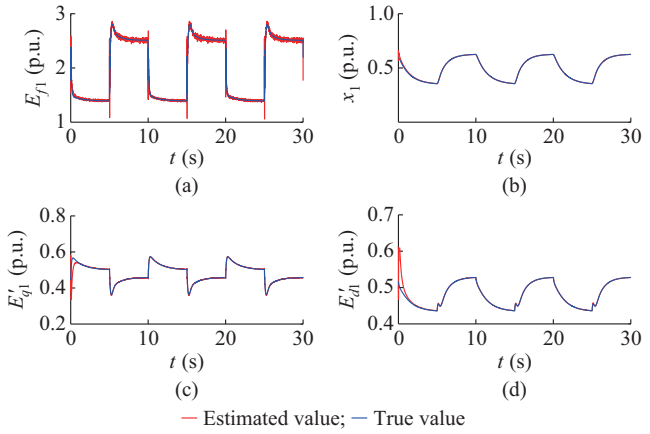

Fig. 11. State variables of 1st generator under rectangular-wave pulse load. (a) E_{f1}. (b) x_1. (c) E'_{q1}. (d) E'_{d1}.

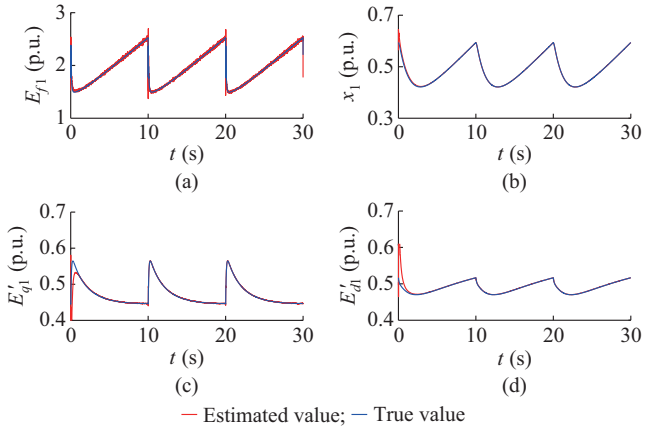

Fig. 12. State variables of 1st generator under triangular-wave pulse load. (a) E_{f1}. (b) x_1. (c) E'_{q1}. (d) E'_{d1}.

From Figs. 9 and 10, it can be seen that there is a relatively large error in estimation near the point of abrupt change of the pulse load. The absolute value of the difference between the estimated value and the true value calculated at each point is the estimation error, and the absolute value of the difference between the measured value and the true value is the measurement error. Taking E_{dc} for example, both of the estimation error and the measurement error of E_{dc} are compared, as shown in Fig. 13.

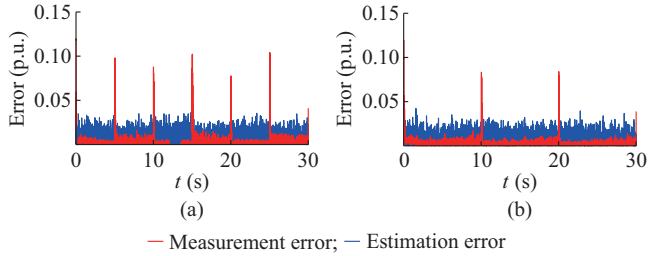

Fig. 13. Comparison of errors of E_{dc}. (a) Under rectangular-wave pulse load. (b) Under triangular-wave pulse load.

According to Fig. 13, the filter achieves a good estimated result on the whole compared with the measured result. Due to a periodic change in the pulse load, the mutation of the system state at the point of abrupt change of the pulse load has a great interference on the accurate estimation of the EKF. The rectangular-wave pulse load suddenly changes two times in each period while the triangular-wave pulse load does only once. Hence, the former has a greater impact on the state estimation. The power change P_m in the sudden-change pulse load is 0.375, with the nominal value as 9 MW. Thus, a large power change can be easily recognized by the measurement system. In Section 5.5 of [6], different affects of the FPN are compared, and many tests show that the filter can obtain better estimation by taking the covariance of the FPN ten times more than that of the measurement noise. For the state variables contained in the measurement equation, large FPN is correspondingly added to their state equation, while other state variables not contained in the measurement equation do not need to be added. The added covariance of the FPN is diag $\{0, 0, 0.001, 0.001, 0, 0, 0.001, 0.001, 0.001\}$. The above-mentioned estimation error and measurement error of E_{dc} after using the FPN are compared, as shown in Fig. 14.

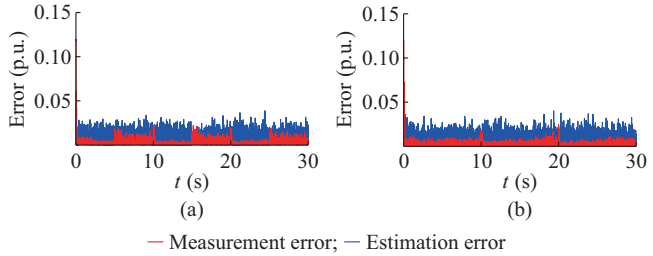

Fig. 14. Comparison of errors of E_{dc} after using FPN. (a) Under rectangular-wave pulse load. (b) Under triangular-wave pulse load.

It is clear that the method of adding FPN can significantly reduce the estimation error at the sudden-change point of the pulse load and can maintain the accuracy of estimation at other positions in the meanwhile. To compare the estimation effects at the sudden-change point of the pulse load, E_{dc} of

the rectangular-wave pulse load is taken for an example. As shown in Fig. 15, a comparison is made between the estimation effects in the two cases where the FPN is added or not to the sudden-change load at 10 s. It is obviously shown in Fig. 15(a) that there is a larger error in the estimation within 0.1 s after the sudden change of pulse load. Then, the filter converges gradually. As shown in Fig. 15(b), after adding the FPN, there is a lower error in the estimation within 0.1 s. After the FPN is removed at 0.1 s, the filter converges gradually.

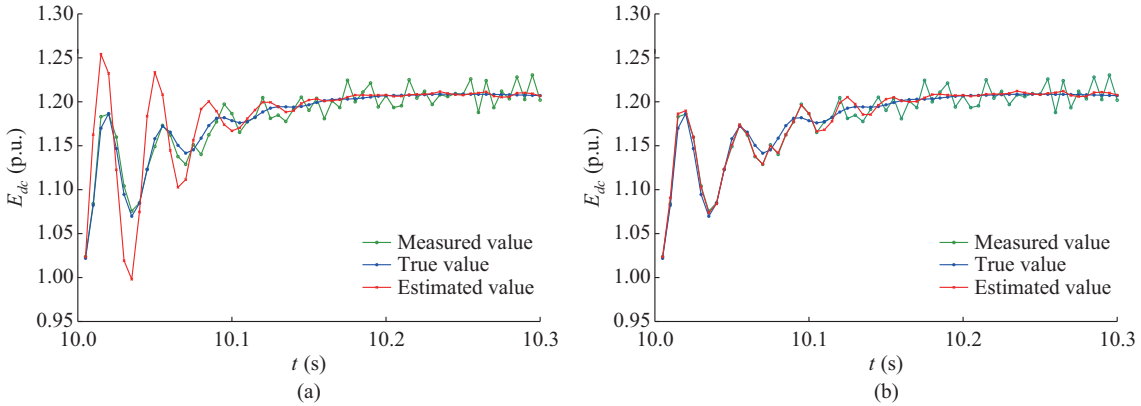

Fig. 15. Estimation under sudden change of pulse load. (a) Without FPN. (b) With FPN.

In the whole range of estimation in Figs. 13 and 14, the error indexes defined in (27) can be used for the intuitive comparison of the effects of state estimation in the case of two kinds of pulse load.

$$\begin{cases} x_{a1} = \dfrac{1}{n}\sum_{i=1}^{n}\left|x_{mi} - x_{ri}\right| \\ x_{a2} = x_{a3} = \dfrac{1}{n}\sum_{i=1}^{n}\left|x_{ei} - x_{ri}\right| \end{cases} \tag{27}$$

where x_{a1} is the index of the measurement errors; x_{a3} and x_{a2} are the indexes of the estimation errors calculated with and without the FPN, respectively; x_{ei} is the estimated value; x_{ri} is the true value; x_{mi} is the measured value; and n is the number of estimation points.

To compare the estimation effects at the sudden-change point of pulse load in Figs. 13 and 14, the point at 10 s is taken for example. According to the same measuring data and initial values, the indexes of estimation errors x_{a5} and x_{a4} in the case of two kinds of pulse load are calculated with and without the FPN from ten tests, respectively. As shown in Tables II and III, the indexes defined above are calculated under the conditions of different measurement noises and different power changes in the sudden-change pulse load. The measurement noise is Gauss white noise with different variances. When different measurement noises are compared, P_m in the sudden-change pulse load is 0.375, and the standard deviation of the measurement noise is 1% when there is a different power change in the sudden-change pulse load. The FPN has a significant effect on the removal of estimation errors at the sudden-change point of pulse load, so x_{a5} is much smaller than x_{a4}, and x_{a3} is improved slightly compared with x_{a2}.

TABLE II
INDEXES OF ERRORS UNDER CONDITIONS OF DIFFERENT MEASUREMENT NOISES

Measurement noise (%)	State variable	Under rectangular-wave pulse load					Under triangular-wave pulse load				
		x_{a1}	x_{a2}	x_{a3}	x_{a4}	x_{a5}	x_{a1}	x_{a2}	x_{a3}	x_{a4}	x_{a5}
1	E_{dc}	0.0082	0.0039	0.0033	0.0896	0.0095	0.0082	0.0031	0.0028	0.0985	0.0086
	I_{dc1}	0.0052	0.0026	0.0022	0.2426	0.0057	0.0052	0.0023	0.0020	0.2468	0.0059
	I_{dc2}	0.0014	0.0014	0.0011	0.0595	0.0020	0.0013	0.0011	0.0010	0.0635	0.0016
2	E_{dc}	0.0166	0.0064	0.0062	0.0936	0.0187	0.0166	0.0058	0.0055	0.1061	0.0185
	I_{dc1}	0.0106	0.0045	0.0041	0.2346	0.0116	0.0102	0.0041	0.0039	0.2707	0.0129
	I_{dc2}	0.0026	0.0016	0.0014	0.0575	0.0031	0.0026	0.0013	0.0012	0.0693	0.0030
4	E_{dc}	0.0333	0.0129	0.0124	0.0961	0.0336	0.0331	0.0106	0.0103	0.1078	0.0370
	I_{dc1}	0.0210	0.0081	0.0076	0.2346	0.0222	0.0202	0.0076	0.0073	0.2583	0.0242
	I_{dc2}	0.0053	0.0023	0.0022	0.0575	0.0060	0.0053	0.0021	0.0020	0.0635	0.0064

From the analysis above, the filter without the use of FPN behaves well in the whole range of estimation, but there will be an unacceptable oscillation, increase or decrease near the point of abrupt change. The use of FPN can reduce the estimation error caused by the periodic change of the pulse load and can improve the stability of the filter. The mean value of the calculation time spent at each estimation point is about 0.03 ms through the calculation on the simulation platform Windows equipped with a 4 GB memory and the fourth-generation CPU i5.

TABLE III
INDEXES OF ERRORS UNDER CONDITIONS OF DIFFERENT POWER CHANGES IN SUDDEN-CHANGE PULSE LOAD

Power change	State variable	Under rectangular-wave pulse load					Under triangular-wave pulse load				
		x_{a1}	x_{a2}	x_{a3}	x_{a4}	x_{a5}	x_{a1}	x_{a2}	x_{a3}	x_{a4}	x_{a5}
0.15	E_{dc}	0.0082	0.0026	0.0024	0.0308	0.0084	0.0083	0.0023	0.0022	0.0367	0.0085
	I_{dc1}	0.0041	0.0021	0.0019	0.0911	0.0044	0.0040	0.0019	0.0016	0.0961	0.0044
	I_{dc2}	0.0011	0.0008	0.0007	0.0224	0.0012	0.0011	0.0008	0.0007	0.0225	0.0012
0.30	E_{dc}	0.0082	0.0034	0.0028	0.0681	0.0085	0.0082	0.0027	0.0025	0.0759	0.0084
	I_{dc1}	0.0048	0.0022	0.0019	0.1926	0.0053	0.0048	0.0021	0.0018	0.1937	0.0058
	I_{dc2}	0.0012	0.0010	0.0009	0.0473	0.0013	0.0012	0.0009	0.0008	0.0495	0.0017
0.45	E_{dc}	0.0082	0.0045	0.0043	0.1150	0.0089	0.0081	0.0033	0.0032	0.1263	0.0087
	I_{dc1}	0.0056	0.0024	0.0022	0.3067	0.0058	0.0054	0.0023	0.0020	0.3254	0.0067
	I_{dc2}	0.0014	0.0011	0.0010	0.0751	0.0017	0.0014	0.0011	0.0010	0.0811	0.0016

V. CONCLUSION

According to the topology and control strategy of the MIPS, this paper presents a dynamic mathematical model of the system. In order to accurately estimate the operation state of the system, a dynamic state estimation method based on the EKF is proposed. The method can be used to deal with complex algebraic variables in the proposed model, which is very applicable for the MIPS. A periodic change in power of the pulse load is called electromagnetic transient process. The time constant which becomes smaller due to a sudden change in the system state will greatly affect the estimation. The use of the FPN at the sudden-change point of pulse load can reduce the interference of the pulse load with the filter, and increase the estimation accuracy and the stability. The proposed dynamic state estimation method is verified by the simulation. Using the FPN, the method can solve the problem that the linearized algorithm of the MIPS model is less reliable when an abrupt change occurs in the pulse load. Thus the estimation accuracy can be improved under the periodic disturbance of pulse load, which will lay a foundation for an accurate dynamic state estimation of the MIPS with pulse load.

REFERENCES

[1] W. Ma, "A survey of the second-generation vessel integrated power system," in *Proceedings of the International Conference on Advanced Power System Automation and Protection*, Beijing, China, Oct. 2011, pp. 1-8.

[2] W. Ma, "The integrated power system in warship," in *Proceedings of the 5th International Marine Electrotechnology Conference*, Shanghai, China, Sept. 2003, pp. 2-7.

[3] *IEEE Recommended Practice for 1 to 35 kV Medium Voltage DC Power Systems on Ships*, IEEE Std. 1709-2010, 2010.

[4] J. F. Hansen and F. Wendt, "History and state of the art in commercial electric ship propulsion, integrated power systems, and future trends," *Proceedings of the IEEE*, vol. 103, no. 12, pp. 2229-2242, Dec. 2015.

[5] G. Wang, R. Xiao, and X. Wu, "Analysis of integrated power system with pulse load by periodic orbit," *IEEE Transactions on Plasma Science*, vol. 47, no. 2, pp. 1345-1351, Feb. 2019.

[6] D. Simon, *Optimal State Estimation: Kalman, H∞, and Nonlinear Approaches*. New York: Wiley, 2006.

[7] J. Zhao, A. Gómez-Expósito, M. Netto *et al*., "Power system dynamic state estimation: motivations, definitions, methodologies, and future work," *IEEE Transactions on Power Systems*, vol. 34, no. 4, pp. 3188-3198, Jul. 2019.

[8] A. G. Phadke and T. Bi, "Phasor measurement units, WAMS, and their applications in protection and control of power systems," *Journal of Modern Power Systems and Clean Energy*, vol. 6, no. 4, pp. 619-629, Jul. 2018.

[9] J. Yang, W. Wu, W. Zheng *et al*., "A sparse recovery model with fast decoupled solution for distribution state estimation and its performance analysis," *Journal of Modern Power Systems and Clean Energy*, vol. 7, no. 6, pp. 1411-1421, Nov. 2019.

[10] G. Anagnostou and B. C. Pal, "Derivative-free Kalman filtering based approaches to dynamic state estimation for power systems with unknown inputs," *IEEE Transactions on Power Systems*, vol. 33, no. 1, pp. 116-130, Jan. 2018.

[11] J. Sun and H. Grotstollen, "Averaged modelling of switching power converters: reformulation and theoretical basis," in *Proceedings of 23rd Annual IEEE Power Electronics Specialists Conference*, Toledo, Spain, Jun.-Jul. 1992, pp. 1165-1172.

[12] N. Xia, H. B. Gooi, S. Chen *et al*., "Decentralized state estimation for hybrid AC/DC microgrids," *IEEE Systems Journal*, vol. 12, no. 1, pp. 434-443, Mar. 2018.

[13] P. Ling, X. Kong, C. Fang *et al*., "Novel distributed state estimation method for the AC-DC hybrid microgrid based on the Lagrangian relaxation method," *The Journal of Engineering*, vol. 2019, no. 18, pp. 4932-4936, Aug. 2019.

[14] X. Kong, Z. Yan, R. Guo *et al*., "Three-stage distributed state estimation for AC-DC hybrid distribution network under mixed measurement environment," *IEEE Access*, vol. 6, pp. 39027-39036, Jul. 2018.

[15] D. Bosich, G. Sulligoi, E. Mocanu *et al*., "Medium voltage DC power systems on ships: an offline parameter estimation for tuning the controllers' linearizing function," *IEEE Transactions on Energy Conversion*, vol. 32, no. 2, pp. 748-758, Jun. 2017.

[16] J. Jatskevich and S. D. Pekarek, "Numerical validation of parametric average-value modeling of synchronous machine-rectifier systems for variable frequency operation," *IEEE Transactions on Energy Conversion*, vol. 23, no. 1, pp. 342-344, Mar. 2008.

[17] S. L. Woodruff, L. Qi, and M. J. Sloderbeck, "Hardware-in-the-loop experiments on the use of propulsion motors to reduce pulse-load system disturbances," in *Proceedings of 2007 IEEE Electric Ship Technologies Symposium*, Arlington, USA, May 2007, pp. 1-7.

[18] H.-F. Li, J. Liang, Z. Yun *et al*., "Optimized operation mode of coordination between the flywheel energy storage and generators for pulsed loads in micro-grid," in *Proceedings of 2017 2nd International Conference on Power and Renewable Energy (ICPRE)*, Chengdu, China, Sept. 2017, pp. 732-736.

[19] P. Kundur, *Power System Stability and Control*. New York: McGraw-Hill Companies, 1994.

[20] R. Wang, Q. Sun, and Y. Gui. "Exponential-function-based droop control for islanded microgrids," *Journal of Modern Power Systems and Clean Energy*, vol. 7, no. 4, pp. 899-912, Jul. 2019.

[21] W. Ma, A. Hu, D. Liu *et al*., "Stability of a synchronous generator with diode-bridge rectifier and back-EMF load," *IEEE Transactions on Energy Conversion*, vol. 15, no. 4, pp. 458-463, Dec. 2000.

[22] M. Sakui and H. Fujita, "An analytical method for calculating harmonic currents of a three-phase diode-bridge rectifier with DC filter," *IEEE Transactions on Power Electronics*, vol. 9, no. 6, pp. 631-637, Nov. 1994.

Runlong Xiao received the B.S. degree in electrical engineering and auto-

mation from Hunan University, Changsha, China, in 2015, and the M.S. degree with the National Key Laboratory of Science and Technology on Vessel Integrated Power System, Navy University of Engineering, Wuhan, China, in 2017, where he is currently pursuing the Ph.D. degree. His current research interest is power system analysis.

Gang Wang received the Ph.D. degree in electrical engineering from Tsinghua University, Beijing, China, in 2008. He is currently a professor and a doctoral tutor with the National Key Laboratory of Science and Technology on Vessel Integrated Power System, Navy University of Engineering, Wuhan, China. His research interests include analysis and control of integrated power system.

Xiaoliang Hao received the B.S. degree in electrical engineering and automation from Shandong University, Jinan, China, in 2015, and the M.S. degree with the National Key Laboratory of Science and Technology on Vessel Integrated Power System, Navy University of Engineering, Wuhan, China, in 2017, where he is currently pursuing the Ph.D. degree. His current research interest is power system analysis.

Renji Huang received the B.S. and the M.S. degrees in information security from Navy University of Engineering, Wuhan, China, in 2016 and 2018, respectively, where he is currently pursuing the Ph.D. degree. His current research interest is power system analysis.

Youxing Xiong received the B.S. and M.S. degrees in information resource management from Wuhan University, Wuhan, China, in 1988 and 2000, respectively. In 1988, she became a lecturer in electrical engineering at the Naval University of Engineering, Wuhan, China, where she has been an associate professor since 2001. Her current research interests include power electronic device modeling and analysis of failure mechanisms.